

# Atomic Ordering in Cubic Bismuth Telluride Alloy Phases at High Pressure

I. Loa,<sup>1,\*</sup> J.-W. G. Bos,<sup>2</sup> R. A. Downie,<sup>2</sup> and K. Syassen<sup>3</sup>

<sup>1</sup>*SUPA, School of Physics and Astronomy, and Centre for Science at Extreme Conditions, The University of Edinburgh, Edinburgh, EH9 3FD, United Kingdom*

<sup>2</sup>*Institute of Chemical Sciences and Centre for Advanced Energy Storage and Recovery, Heriot-Watt University, Edinburgh, EH14 4AS, United Kingdom*

<sup>3</sup>*Max-Planck-Institut für Festkörperforschung, Heisenbergstr. 1, 70569 Stuttgart, Germany*

(Dated: June 9, 2016)

Pressure-induced transitions from ordered intermetallic phases to substitutional alloys to semi-ordered phases were studied in a series of bismuth tellurides. Using angle-dispersive x-ray diffraction, the compounds  $\text{Bi}_4\text{Te}_5$ ,  $\text{BiTe}$ , and  $\text{Bi}_2\text{Te}$  were observed to form alloys with the disordered body-centered cubic (bcc) crystal structure upon compression to above 14–19 GPa at room temperature. The  $\text{BiTe}$  and  $\text{Bi}_2\text{Te}$  alloys and the previously discovered high-pressure alloys of  $\text{Bi}_2\text{Te}_3$  and  $\text{Bi}_4\text{Te}_3$  were all found to show atomic ordering after gentle annealing at very moderate temperatures of  $\sim 100^\circ\text{C}$ . Upon annealing,  $\text{BiTe}$  transforms from the bcc to the B2 (CsCl) crystal structure type, and the other phases adopt semi-disordered variants thereof, featuring substitutional disorder on one of the two crystallographic sites. The transition pressures and atomic volumes of the alloy phases show systematic variations across the  $\text{Bi}_m\text{Te}_n$  series including the end members Bi and Te. First-principles calculations were performed to characterize the electronic structure and chemical bonding properties of B2-type  $\text{BiTe}$  and to identify the driving forces of the ordering transition. The calculated Fermi surface of B2-type  $\text{BiTe}$  has an intricate structure and is predicted to undergo three topological changes between 20 and 60 GPa.

PACS numbers: 61.50.Ks, 61.66.Dk, 62.50.-p, 71.20.Lp

## I. INTRODUCTION

Bismuth tellurides,  $\text{Bi}_m\text{Te}_n$ , are a class of intermetallic compounds with intriguing physical properties.  $\text{Bi}_2\text{Te}_3$  is one of the best bulk thermoelectric materials for operation near room temperature;<sup>1</sup> it becomes superconducting under pressure;<sup>2–6</sup> it has been reported to undergo a pressure-induced electronic topological (Lifshitz) transition,<sup>3,7–10</sup> and it has recently attracted much interest in the context of topological insulators.<sup>11–13</sup> Like  $\text{Bi}_2\text{Te}_3$ , the compound  $\text{Bi}_4\text{Te}_3$  also becomes superconducting under pressure<sup>14</sup> after turning from a narrow-bandgap semiconductor into a metal. The structural changes in  $\text{Bi}_2\text{Te}_3$  and  $\text{Bi}_4\text{Te}_3$  under compression have been studied previously, and both intermetallic compounds were observed to transform to alloys with a disordered body-centered-cubic (bcc) crystal structure above  $\sim 15$  GPa at room temperature.<sup>14–16</sup> The two materials are members of the infinitely adaptive series of compounds with compositions  $(\text{Bi}_2)_\mu \cdot (\text{Bi}_2\text{Te}_3)_\nu$ , and their crystal structures at ambient conditions are all superlattice structures consisting of hexagonal  $\text{Bi}_2$  and  $\text{Bi}_2\text{Te}_3$  blocks.<sup>13,17,18</sup> The materials with compositions near  $\mu:\nu = 2:1$  (e.g.  $\text{Bi}_2\text{Te}$ ) are promising  $p$ -type thermoelectrics.<sup>17,18</sup>

Here we show that the existence of high-pressure bcc alloy phases is a common feature across the  $\text{Bi}_m\text{Te}_n$  series, and that these phases are thermally rather unstable — they have a propensity for atomic ordering upon gentle annealing at only  $\sim 100^\circ\text{C}$  under pressure. During annealing, the  $\text{BiTe}$  compound adopts the fully-ordered B2 (CsCl-type) structure, and the other compounds semi-disordered variants thereof. First-principles electronic structure calculations are used to investigate the chemical bonding and electronic structure of B2-type  $\text{BiTe}$  and to gain insight on the driving forces for the ordering transition.

## II. METHODS

The compounds  $\text{Bi}_4\text{Te}_5$ ,  $\text{BiTe}$ ,  $\text{Bi}_4\text{Te}_3$ , and  $\text{Bi}_2\text{Te}$  were synthesized as polycrystalline pellets by solid-state reaction from the elements as described previously.<sup>17,18</sup> A single crystal of  $\text{Bi}_2\text{Te}_3$  was provided by D. L. Sun and C. T. Lin (Max-Planck-Institut für Festkörperforschung, Stuttgart). Each material was manually ground to a fine powder and loaded into diamond anvil cells (DACs) for high-pressure generation. In the majority of the experiments, condensed helium was used as the pressure transmitting medium; some additional experiments that focussed on the effect of annealing the samples at  $\sim 100^\circ\text{C}$  were performed with nitrogen or a 4:1 methanol-ethanol mixture as the pressure transmitting medium. Pressures were determined with the ruby fluorescence method using the calibration of Ref. 19.

Monochromatic powder x-ray diffraction patterns were measured in the Debye-Scherrer geometry on beamline ID09a of the European Synchrotron Radiation Facility (ESRF) and beamline I15 of Diamond Light Source (DLS), UK. Monochromatic x-rays of wavelength  $\lambda \approx 0.415 \text{ \AA}$  were focused to a spot size of  $\sim 20 \mu\text{m}$  at the sample, and the two-dimensional diffraction images were recorded with a mar555 and a Perkin Elmer XRD1621 flat panel detector at the ESRF and DLS, respectively. The DACs were rotated by  $\pm 3\text{--}5^\circ$  during the exposure to improve the powder averaging. The diffraction images were integrated azimuthally with the Fit2D software<sup>20</sup> to yield conventional intensity vs  $2\Theta$  diffraction diagrams, and then analyzed with the Rietveld method using the program Jana2006.<sup>21</sup>

Electronic structure calculations of  $\text{BiTe}$  were performed in the framework of density functional theory (DFT) and the full-potential augmented-plane-wave + local orbital (APW+lo) approach as implemented in the WIEN2K<sup>22</sup> and ELK<sup>23</sup> codes.

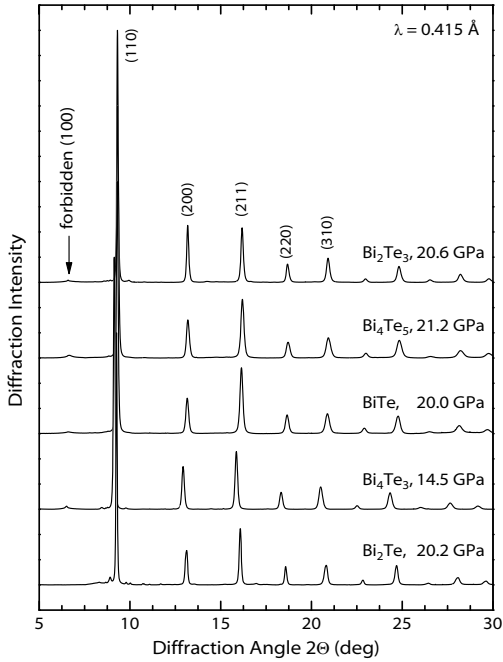


FIG. 1. Powder x-ray diffraction patterns of the disordered-bcc phases of  $\text{Bi}_m\text{Te}_n$  after compression at room temperature. All phases except  $\text{Bi}_2\text{Te}$  show a weak feature at the position of the (100) reflection, which is absent in an ideal bcc phase. Note that the reflection intensities of  $\text{Bi}_2\text{Te}_3$  have been affected by preferred orientation of the powder sample, and the very weak features near  $9^\circ$  originate from the nitrogen pressure medium or the remainder of a lower-pressure phase.

The  $5d$ ,  $6s$ , and  $6p$  orbitals of Bi and the  $4d$ ,  $5s$ , and  $5p$  orbitals of Te were treated as valence states. Exchange and correlation effects were treated with the revised generalized gradient approximation for solids (PBEsol).<sup>24</sup> Spin-orbit coupling was previously found to have a significant effect<sup>25,26</sup> on the electronic structure of  $\text{Bi}_2\text{Te}_3$  and was therefore included in the present calculations. Regular Monkhorst-Pack grids of  $k$ -points, typically  $20 \times 20 \times 20$ , were used for the Brillouin-zone sampling.<sup>27</sup> The electronic band structure and density of states obtained with the two codes were in complete agreement. To quantify the charge transfer between Bi and Te in  $\text{BiTe}$ , the `CRITIC` code<sup>28</sup> was used to perform Bader analyses of the charge density distribution obtained with Wien2k. The electron localization function (ELF)<sup>29,30</sup> was calculated using the ELK code.

### III. RESULTS AND DISCUSSION

#### A. Disordered bcc Phases

All five compounds were compressed at room temperature, and after one or more phase transitions, each of them was found to transform to a phase with the diffraction pattern characteristic of a bcc crystal, as illustrated in Figure 1. This suggests that disordered bcc alloy phases at high pressure are a

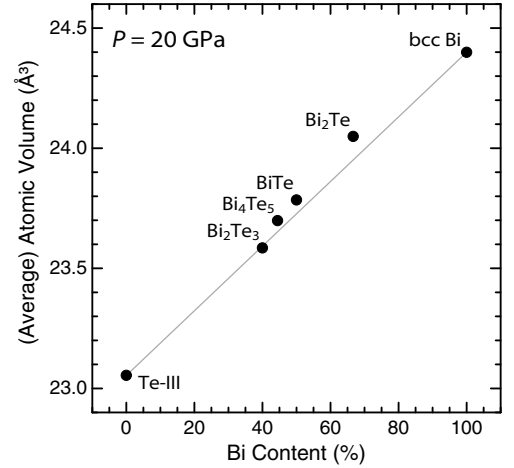


FIG. 2. Average atomic volumes of the bcc alloy phases of  $\text{Bi}_m\text{Te}_n$  and atomic volumes of Bi and Te at 20 GPa.<sup>31,32</sup> Note that the crystal structure of Te at 20 GPa is incommensurately-modulated body-centered monoclinic (Te-III).<sup>32</sup> The straight line indicates a linear variation of the volume with composition according to Vegard's law.

general feature of the compounds across the Bi-Te system. With the exception of the  $\text{Bi}_2\text{Te}$  pattern, the diffraction patterns show a very weak feature at the position of the (100) reflection, which is forbidden for a monatomic or ideal bcc phase. In the alloy phases, the presence of this reflection indicates a slight deviation from a completely random distribution of the Bi and Te atoms, i.e., the occurrence of some short-range correlations. Overall, however, Rietveld analysis of the diffraction patterns confirms them to be consistent with the model of disordered Bi-Te alloys as reported previously for  $\text{Bi}_2\text{Te}_3$  and  $\text{Bi}_4\text{Te}_3$  (Refs. 14 and 15).

Figure 2 shows the average atomic volumes for the alloy phases at 20 GPa as a function of composition. The atomic volumes of Bi and Te at the same pressure are shown for comparison. Note that Bi adopts the bcc structure at this pressure, whereas Te has an incommensurately-modulated body-centered monoclinic structure<sup>32</sup> and transforms to bcc only at  $\sim 29$  GPa. There is a continuous evolution of the atomic volume across the series with only a slight deviation from Vegard's law.  $\text{Bi}_2\text{Te}$  shows the most notable deviation (0.4%). Einaga *et al.*<sup>15</sup> performed a similar analysis for  $\text{Bi}_2\text{Te}_3$  between 23 and 30 GPa and concluded that there is a substantial deviation from Vegard's law, which was attributed to "remaining strong ionic-covalent bonds". The important difference between the two analyses is that Einaga *et al.* used an extrapolation of the equation of state of bcc Te<sup>33</sup> to lower pressures whereas we used the actual atomic volume<sup>32</sup> of Te at 20 GPa as a reference. The former has the advantage of referring to the same crystal structure for the whole series of compositions, whereas the latter uses only the experimentally observed volumes, irrespective of the crystal structure. We should note that the deviation from Vegard's law in Einaga's analysis becomes significantly smaller if, instead of the of bcc Te equation-of-state data by Parthasarathy and Holzapfel,<sup>33</sup> one uses the more recent data by Hejny and McMahon.<sup>32</sup>

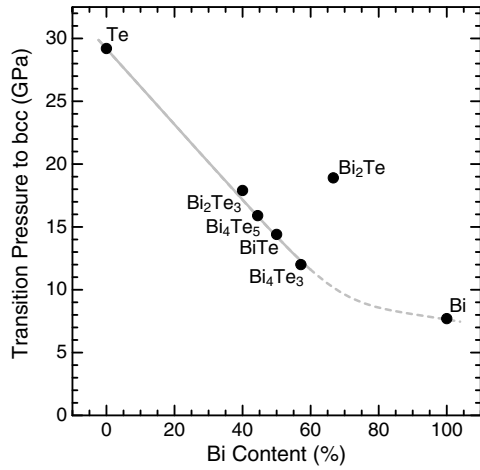


FIG. 3. Transition pressures to the bcc alloy phases of  $\text{Bi}_m\text{Te}_n$  during compression as a function of composition. At the given pressures, approximately 50% of each powder sample had transformed from the lower-pressure to the bcc phase. The transition pressures for Te and Bi are from Refs. 32 and 34, respectively.

Overall, we see little evidence for a significant deviation from Vegard’s law. The nature of the bonding in the Bi-Te alloys at high pressure, on the other hand, remains a pertinent question, to which we will return later.

Figure 3 illustrates that the pressure at which the transition to the bcc phase occurs varies continuously across the series of compositions — with the notable exception of  $\text{Bi}_2\text{Te}$  for which the transition pressure is  $\sim 9$  GPa higher than expected from the overall trend. The determination of the crystal structures that precede bcc  $\text{Bi}_2\text{Te}$  at lower pressure is in progress, and the results, that may shed some light on this anomaly, will be reported elsewhere.

### B. Semi-disordered B2-Type Phases

In our initial experiments on  $\text{Bi}_2\text{Te}_3$  we attempted to sharpen the diffraction pattern of a phase at 17 GPa (phase III in the notation of Refs. 15, 16, and 35) by annealing the sample in the DAC gently at  $120^\circ\text{C}$ . During this treatment, the sample transformed to a cubic phase, but not the bcc alloy phase discussed above. Rather, a closely-related phase with superstructure reflections in the diffraction pattern was observed, as illustrated in Fig. 4. Evidently, the thermal treatment induced some atomic ordering, and the same effect was subsequently observed also for  $\text{BiTe}$ ,  $\text{Bi}_4\text{Te}_3$ , and  $\text{Bi}_2\text{Te}$ . ( $\text{Bi}_5\text{Te}_4$  has not yet been tested for this effect.) The diffraction patterns with the superstructure reflections can be indexed using a simple cubic unit cell and lattice parameters similar to those of the corresponding bcc phases.

As it is not possible to obtain an ordered structure of  $\text{Bi}_2\text{Te}_3$  on the basis of a cubic unit cell containing only two atoms, we considered superstructures that are compatible with the given stoichiometry, such as the cubic  $\text{Pr}_2\text{C}_3$  structure type, but none of these was consistent with the observed diffrac-

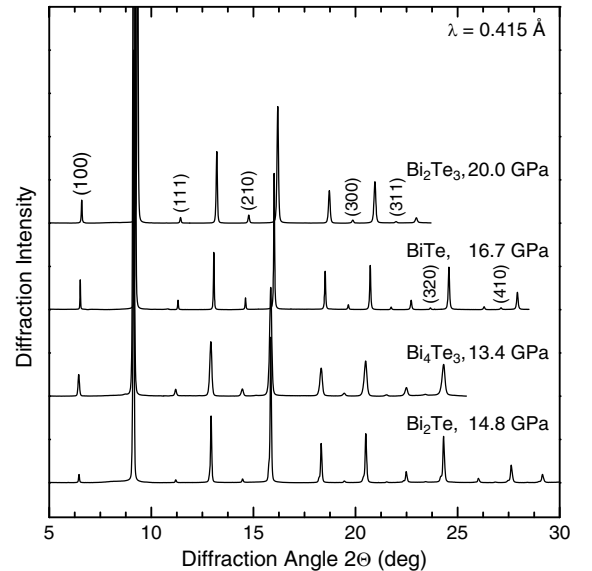


FIG. 4. Powder x-ray diffraction patterns of the partially-ordered B2-type phases of  $\text{Bi}_m\text{Te}_n$  after compression at room temperature and subsequent annealing at  $100^\circ\text{C}$  ( $\text{BiTe}$ ,  $\text{Bi}_4\text{Te}_3$ ,  $\text{Bi}_2\text{Te}$ ) or  $120^\circ\text{C}$  ( $\text{Bi}_2\text{Te}_3$ ). Miller indices marks the superstructure reflections.

tion pattern. We also considered the monoclinic structure “nine/ten-fold  $C2/m$ ” proposed by Zhu *et al.*,<sup>16</sup> which they identified in their structure search calculations as the stable phase above 16 GPa. This structure model produces a diffraction pattern similar to that observed for  $\text{Bi}_2\text{Te}_3$  after annealing, but with the large monoclinic unit cell containing 20 atoms, it produces also a large number of low-intensity reflections that are not observed experimentally. Zhu *et al.* interpreted this structure as an approximation of the disordered bcc alloy structure. Careful inspection of the “nine/ten-fold  $C2/m$ ” structure reveals it to be actually more closely related to the B2 (CsCl) structure type, with 1/5 of the rows of Bi atoms along the cubic (110) direction being replaced with rows of Te atoms (in an ordered fashion). Building on this realization and taking into account the substitutional disorder before annealing, we determined the structures of the annealed  $\text{Bi}_m\text{Te}_n$  phases to be semi-disordered variants of the B2 structure type. In each case, one crystallographic site of the B2 unit cell is essentially occupied by the majority element only, whereas the other site is randomly occupied by either element under the constraint of the overall stoichiometry. For  $\text{Bi}_2\text{Te}_3$ , one site is then, ideally, fully occupied by Te and the other site has a mixed occupancy by Bi and Te at a ratio of 80:20 as illustrated in Fig. 5.

Figure 6 shows the result of a Rietveld refinement for the diffraction pattern of annealed  $\text{Bi}_2\text{Te}_3$  at 20 GPa on the basis of the semi-disordered B2 structure, which yields an excellent fit with residuals of  $R_p = 1.5\%$  and  $R_{wp} = 2.5\%$ . One site is mostly occupied by the majority Te with a Bi:Te ratio of 6:94(1) and the other site consequently with a Bi:Te ratio of 74:26(1). This sample was annealed for 26 h at  $120^\circ\text{C}$ , but we found that much shorter annealing can already induce significant ordering. This is illustrated in Fig. 7 which shows

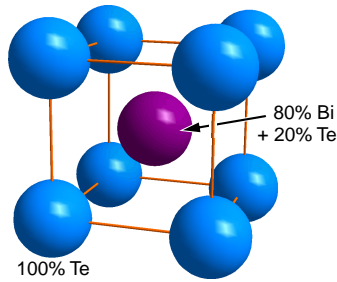


FIG. 5. (Color online) Idealized crystal structure of semi-disordered B2-type  $\text{Bi}_2\text{Te}_3$  with full occupation of one crystallographic site and mixed occupation of the other.

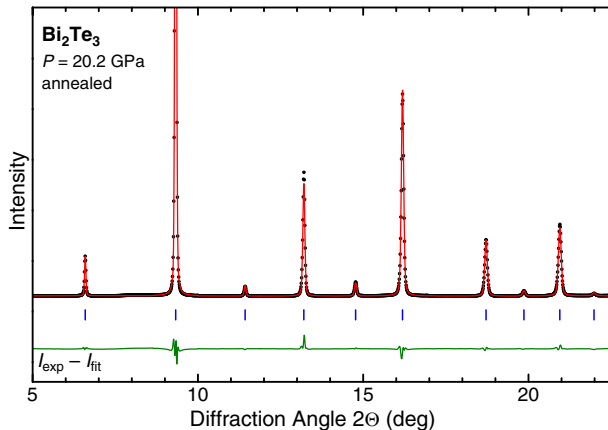


FIG. 6. (Color online) Rietveld refinement for semi-disordered B2-type  $\text{Bi}_2\text{Te}_3$  at 20.0 GPa after 26 h of annealing at 120°C. The dots and the solid line in the upper part show the measured and fitted diffraction intensities, respectively. The tick marks show the calculated peak positions, and the bottom curve the difference between measured and fitted intensities.

the result of a Rietveld refinement for  $\text{Bi}_2\text{Te}$  at 14.8 GPa after only 2 h of annealing at 100°C. The Rietveld fit (with residuals of  $R_p = 2.2\%$  and  $R_{wp} = 3.0\%$ ) yields Bi:Te ratios of 90:10(2) and 41:59(2) for the two sites. This figure illustrates furthermore that we found  $\text{Bi}_2\text{Te}$  to precipitate a small amount of Bi ( $\sim 6\%$ ) into a second phase. The bcc Bi phase has a lattice parameter slightly larger<sup>31</sup> than that of B2-type  $\text{Bi}_2\text{Te}$  at this pressure, so that it produces shoulders on the lower-angle sides of the  $\text{Bi}_2\text{Te}$  diffraction peaks as shown in the inset to Fig. 7.

Table I summarizes the conditions under which four  $\text{Bi}_m\text{Te}_n$  phases were annealed to transform them from their alloys to the semi-disordered B2 phases, together with the relative occupancies of the two sites as a measure of the ordering. The  $\text{BiTe}$  sample was annealed three times in succession. The first treatment at a relatively high pressure of 25 GPa (11 GPa above the transition pressure to bcc) produced only rather limited ordering. Two subsequent annealing steps at lower pressures of 17–18 GPa eventually produced almost complete (97%) ordering. Altogether, we found that thermal treatment at moderate temperatures of 100–120°C causes the high-pressure Bi-Te bcc alloy phases to transform readily to semi-

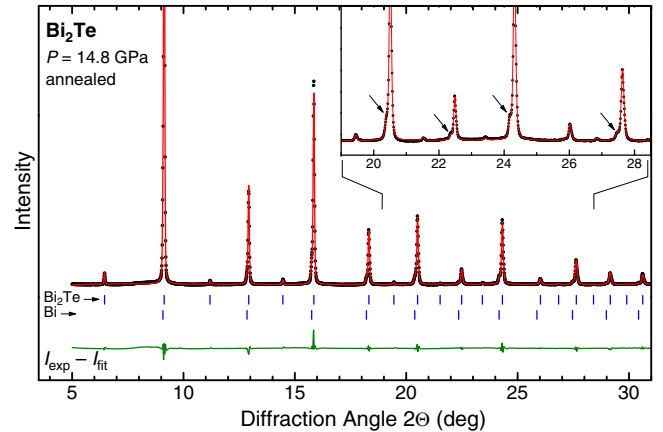


FIG. 7. (Color online) Rietveld refinement for  $\text{Bi}_2\text{Te}$  at 14.8 GPa after 2 h of annealing at 100°C. Two phases were refined simultaneously: semi-disordered B2-type  $\text{Bi}_2\text{Te}$  and bcc Bi. The bcc Bi phase produces shoulders on the lower-angle sides of some peaks as highlighted in the inset. The dots and the solid line in the upper part show the measured and fitted diffraction intensities, respectively. The tick marks show the calculated peak positions for the two phases, and the bottom curve the difference between measured and fitted intensities.

TABLE I. Atomic ordering in B2-type  $\text{Bi}_m\text{Te}_n$  after thermal annealing. The temperature, duration and final pressure of the thermal treatment are indicated by  $T$ ,  $\Delta t$ , and  $P$ , respectively. The Bi:Te ratios or relative occupancies of the two sites were determined with Rietveld refinements. Site 1 is the site of the majority element, and its Bi:Te ratio represents the degree of ordering. The  $\text{BiTe}$  sample was annealed three times in succession, with each step as indicated.

Phase	Annealing			Bi:Te ratios	
	$T$ (°C)	$\Delta t$ (h)	$P$ (GPa)	site 1	site 2
$\text{Bi}_2\text{Te}_3$	120	26	18	6:94(1)	74:26(1)
$\text{BiTe}$	100	25	24	26:74(2)	74:26(2)
	100	+42	18	91:9(1)	9:91(1)
	100	+92	17	97:3(1)	3:97(1)
$\text{Bi}_4\text{Te}_3$	100	16	14	90:10(2)	24:76(2)
$\text{Bi}_2\text{Te}$	100	2	15	90:10(2)	41:59(2)

ordered phases of the B2 structure type. Prolonged annealing of  $\text{BiTe}$  led to nearly complete ordering, and it appears likely that for the other phases a higher degree of ordering could also be obtained with prolonged annealing.

The phases with compositions other than 1:1  $\text{BiTe}$  could potentially order further by adopting superlattice structures of the B2 type, e.g. partially disordered variants of the structures of Heusler compounds. However, careful inspection of the patterns in Fig. 4 yields no evidence for  $(\frac{1}{2} \frac{1}{2} \frac{1}{2})$  superlattice reflections that would be indicative of structure types such as  $L2_1$ ,  $\text{DO}_3$  or  $\text{Y}$  (Ref. 36 and 37).

Intermetallic compounds are well known to exhibit widely varying degrees of atomic order — from completely disordered alloys to fully ordered compound phases — depending on stoichiometry, temperature, and thermal and mechanical treatment.<sup>38</sup> The semi-disordered B2-type phases observed

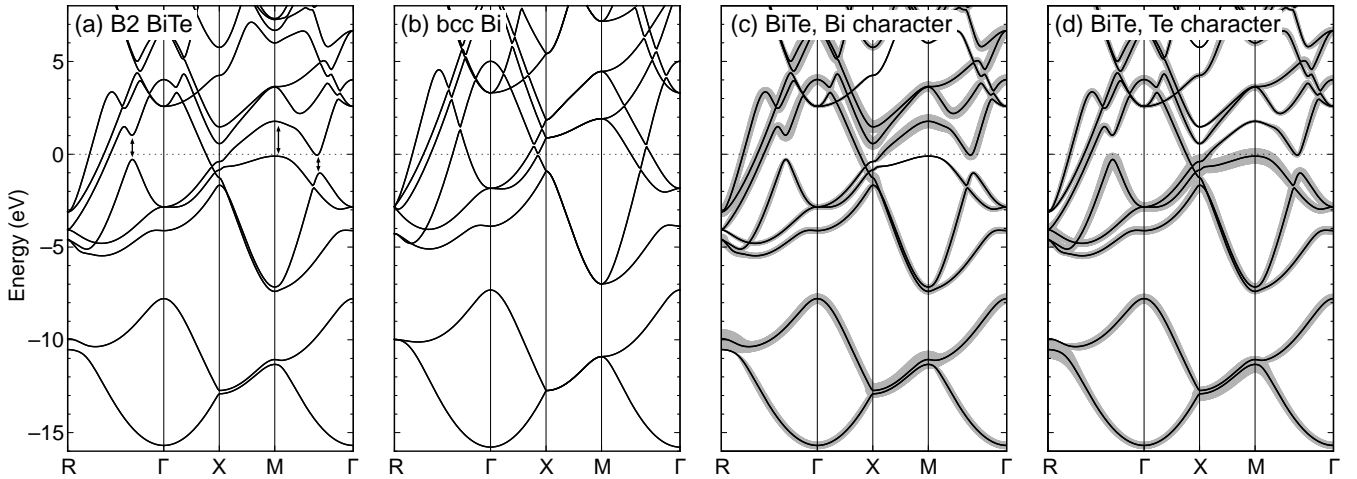


FIG. 8. Calculated electronic band structures of (a) B2-type BiTe and (b) bcc Bi for cubic unit cells with a lattice parameter of 3.623 Å, corresponding to the experimental density of bcc BiTe at 20 GPa. The calculated pressure for B2-type BiTe at this density is 18.5 GPa. To facilitate the comparison between B2-type BiTe and bcc Bi, the band structure for the latter is not shown with respect to the usual bcc Brillouin zone, but rather with respect to the same simple cubic Brillouin zone as for B2-type BiTe. (c) Bi character and (d) Te character of the electronic bands in BiTe at 18.5 GPa are shown by the widths of the gray bands (“fat bands”), as quantified by the partial charges of the band states in the atomic spheres. The most notable differences between (c) and (d) can be seen for states close to the Fermi level, e.g. around the M point.

here are reminiscent of semi-disordered B2-type phases observed in some  $X_2YZ$  Heusler compounds, e.g.  $\text{Co}_2\text{FeAl}$  at high temperature,<sup>39</sup> where the X atoms occupy one site of the B2 structure and the Y and Z atoms randomly occupy the other site.<sup>36</sup> Intermetallic phases generally have a tendency to long-range order.<sup>38</sup> To obtain an alloy, atomic ordering must be prevented, typically by quenching a high-temperature disordered phase, or destroyed, e.g. by cold working. Although it is therefore to be expected to observe ordering in the Bi-Te phases at elevated temperatures, it is surprising to observe it at such relatively low temperatures of only  $\sim 100^\circ\text{C}$ . It is therefore possible that atomic ordering will occur already at room temperature on a longer time scale. In other words, the Bi-Te alloy phases may show signs of aging.

Atomic disorder in intermetallic compounds is well documented to affect their physical properties, e.g. the magnetism in Heusler compounds,<sup>36</sup> the mechanical properties of structural alloys,<sup>38</sup> or the superconductivity in A15 intermetallics.<sup>38</sup> Superconductivity in  $\text{Bi}_2\text{Te}_3$  and  $\text{Bi}_4\text{Te}_3$  has been observed in the pressure range where their cubic alloy phases exist.<sup>5,14</sup> The existence of both alloy and semi-ordered Bi-Te phases therefore needs to be taken into account in investigations of their physical properties, in particular in electronic structure calculations.

### C. Electronic Structure and Chemical Bonding in BiTe

The fully-ordered B2-type BiTe phase provides an ideal starting point for electronic structure calculations, which allow us to gain insight on the nature of its chemical bonding and the forces that drive the atomic ordering. Figure 8(a) shows the calculated band structure of B2-type BiTe at the experimental density of bcc BiTe at 20 GPa. Spin-orbit coupling

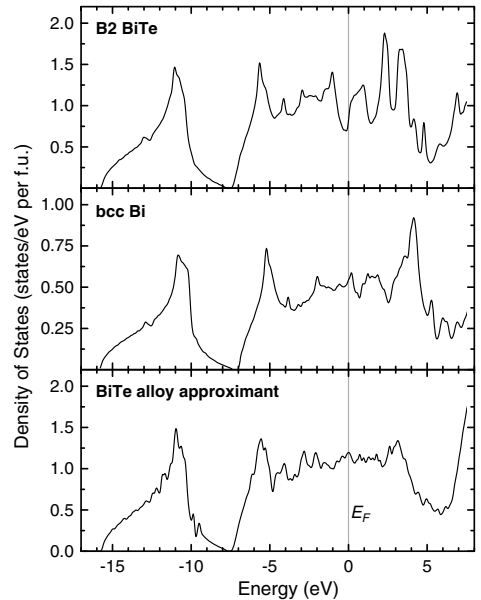


FIG. 9. Calculated electronic density of states of B2-type BiTe at a calculated pressure of 18.5 GPa (lattice parameter  $a = 3.623$  Å), of bcc Bi, and of a BiTe alloy approximant. The same atomic density was used in all three calculations. The Fermi level  $E_F$  was set to be 0.

was included in all calculation and was found to produce significant band splittings, in agreement with earlier studies<sup>25,26</sup> on  $\text{Bi}_2\text{Te}_3$ . In the calculation, BiTe is metallic at this pressure, which is in line with the observation that the band gap in  $\text{Bi}_2\text{Te}_3$  closes at pressures of 2–5 GPa, depending on the sample and pressure/stress conditions.<sup>6,40</sup> The BiTe band structure is similar to that of bcc Bi at the same atomic density [Fig. 8(b)]. The most notable difference is the occurrence

of additional band splittings for BiTe, as indicated by arrows in Fig. 8(a). This reduces the number of bands crossing the Fermi level and produces a suppression in the electronic density of states — a pseudogap — near the Fermi level as illustrated in Fig. 9. This suppression is absent for bcc Bi and, more importantly, for an approximant of the BiTe alloy, which we modeled as a  $2 \times 2 \times 2$  supercell of B2-type BiTe with a random distribution of the eight Bi and eight Te atoms. The result is a slightly reduced band structure contribution to the total energy of the ordered phase in comparison to the alloy. This illustrates at a fundamental level the discussion in the previous section on the effect of atomic disordering on the electronic properties.

Analysis of the partial charges from the individual band states shows that the lower-energy components of the split bands near the Fermi level have predominantly Te character, and the higher-energy components predominantly Bi character [Fig. 8(c,d)]. This indicates a charge transfer from Bi to Te, which is in keeping with Te having a slightly higher electronegativity than Bi (2.1 vs 2.02 on the revised Pauling scale<sup>41</sup>). To quantify the charge transfer, we performed a Bader (“Atoms in Molecules”) analysis<sup>42,43</sup> of the charge density distribution. In this analysis, the unit cell is divided into regions whose boundaries are defined by minima in the charge density. More precisely, at any point on the dividing boundaries, the gradient of the charge density is parallel to the boundary or zero. This provides an unambiguous partitioning of the unit cell into atomic basins, and by integrating the charge within these basins one can quantify the charge transfer between atoms. For BiTe at  $\sim 20$  GPa, the Bader analysis indicates a significant charge transfer from Bi to Te of approximately  $0.44 e$ . The charge transfer depends only weakly on the pressure and decreases with increasing pressure to  $0.40 e$  at 100 GPa.

The chemical bonding and charge transfer between Bi and Te have been analyzed in several studies on  $\text{Bi}_2\text{Te}_3$  at normal pressure.<sup>16,25,44,45</sup> The  $\text{Bi}_2\text{Te}_3$  crystal structure can be regarded as a repeating sequence of “quintuple layers” that comprise five atomic layers, Te(1)–Bi–Te(2)–Bi–Te(1), where Te(1) and Te(2) denote the two crystallographic sites occupied by Te. The bonding within the quintuple layers is of mixed covalent-ionic type, whereas the bonding between the quintuple layers is of van-der-Waals type. The degree of ionicity is generally difficult to quantify, and model-dependent, and the results of several studies vary correspondingly. The combined DFT and tight-binding calculations by Mishra *et al.*<sup>25</sup> gave ionic charges of  $\text{Bi}_2^{0.7+} \text{Te}(1)_2^{0.5-} \text{Te}(2)^{0.35-}$ . An earlier tight-binding model by Pecheur and Toussaint<sup>45</sup> had indicated ionic charges about 50% lower than those obtained by Mishra *et al.* On the other hand, Zhu *et al.*<sup>16</sup> recently reported ionic charges of  $\text{Bi}_2^{0.75+} \text{Te}(1)_2^{0.05-} \text{Te}(2)^{1.39-}$  (on the basis of DFT calculations and Bader analysis), which suggested a strong charge disproportionation between the two Te sites. They furthermore reported the charge transfer from Bi to Te to increase with increasing pressure. It is therefore interesting to note that the charge transfer obtained here for cubic BiTe is significantly lower than those reported by Zhu *et al.* for the layered ambient-pressure and three high-pressure phases of  $\text{Bi}_2\text{Te}_3$ ,

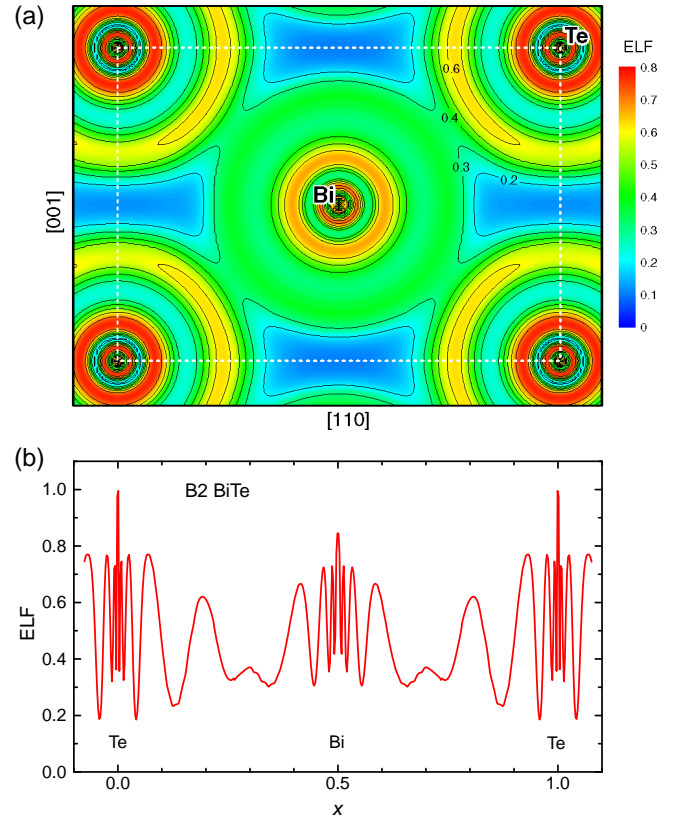


FIG. 10. (Color online) Calculated electron localization function of B2-type BiTe at a calculated pressure of 18.5 GPa (lattice parameter  $a = 3.623$  Å). (a) ELF in the (110) plane. The unit cell edges are indicated by the white dotted lines. (b) ELF along the body diagonal  $(x, x, x)$  of the cubic unit cell.

and their pressure dependences are also at variance.

To further address the question whether any significant covalent contribution to the chemical bonding is still present at high pressure in the cubic phases (as suggested in Refs 15 and 16), we have calculated the electron localization function (ELF)<sup>29,30</sup> for BiTe. The results for B2-type BiTe are shown in Fig. 10. The upper panel shows the ELF in the (110) plane that passes through four Te atoms at the corners of the unit cell and the Bi atom in the center. There is no indication of a local maximum of the ELF along the Bi–Te line, and hence no indication of directional, covalent bonding between Bi and Te. The oscillations in the ELF in Fig. 10(b) represent merely the electronic shell structure of Bi and Te.

The overall picture emerging from these calculations is thus one where the mixed covalent-ionic plus van-der-Waals bonding found in the bismuth tellurides at ambient conditions gives way to metallic bonding with a significant ionic component at high pressures of  $\sim 20$  GPa. The charge transfer from Bi to Te is rather insensitive to further increase in pressure. We consider the charge transfer to be the driving force behind the thermally-induced atomic ordering. Firstly, ordering of the Bi and Te ions reduces the Madelung energy. The semi-ordered phases for the compositions other than BiTe represent the most-ordered configurations that can be achieved within



the bcc/B2 structure type under the constraint of the given stoichiometry. Secondly, the ion ordering in BiTe causes a suppression of the electronic density of states near the Fermi level, and hence a lowering of the band structure contribution to the total energy. It is not clear at present to what extent this second effect contributes to the formation of the semi-ordered phases.

#### D. Fermi Surface of BiTe and Topological Changes

Figure 8(a) shows that several electronic bands cross the Fermi level in B2-type BiTe and that there are three band extrema in close proximity to the Fermi level. These extrema arise from the band splittings marked by arrows in Fig. 8(a), which are due to the ionicity in BiTe as discussed above. The Fermi surface thus comprises several sheets, and its topology can be expected to change with pressure when band extrema cross the Fermi level. Figure 11(a) shows the calculated Fermi surface of B2-type BiTe at the same density as for the band structure in Fig. 8(a). It consists of three electron pockets nested inside one another and centered around the R point as well as a tube-like feature with necks at the X points. With increasing pressure, the band minimum along  $\Gamma$ -M, the maximum along  $\Gamma$ -R, and the maximum at M cross the Fermi level at calculated pressures of 29, 38, and 47 GPa, respectively. The associated changes in the topology of the Fermi surface are illustrated in Fig. 11(b). The tube-like feature breaks up into pockets centered on the X points, and additional pockets appear upon further compression. We expect these Fermi surface features to be sensitive not only to changes in pressure but also to atomic displacements, which may give rise to interesting electron-phonon coupling effects.

We should note that although we did not investigate the stability of cubic bcc/B2-type BiTe at pressures above 25 GPa, we expect it to be stable over a wide pressure range. B2-type phases are generally rather stable under compression, and bcc Bi has been reported to be stable to at least 222 GPa (Ref. 31), bcc Te to 97 GPa (Ref. 46), and the  $\text{Bi}_2\text{Te}_3$  bcc alloy phase to at least 52 GPa (Ref. 16).

#### IV. CONCLUSIONS

We have shown that the formation of alloy phases at high pressure appears to be a common feature across the series of  $\text{Bi}_m\text{Te}_n$  compounds. The alloy phases were found to be thermally unstable and to adopt semi-disordered B2/CsCl-type structures after gentle annealing, but not the superlattice structures known from Heusler compounds. The atomic ordering must be expected to affect the physical properties of the alloy phases, e.g. superconductivity.<sup>2-6,14,47</sup> Electronic structure calculations indicate a significant charge transfer of  $\sim 0.4 e$  from Bi to Te in B2-type BiTe. The ionic contribution to the bonding favors atomic ordering and thus the transition from alloy to ordered compound. Another contribution is the lowering of the band structure contribution to the total energy due to a suppression of the electronic density of states near the Fermi

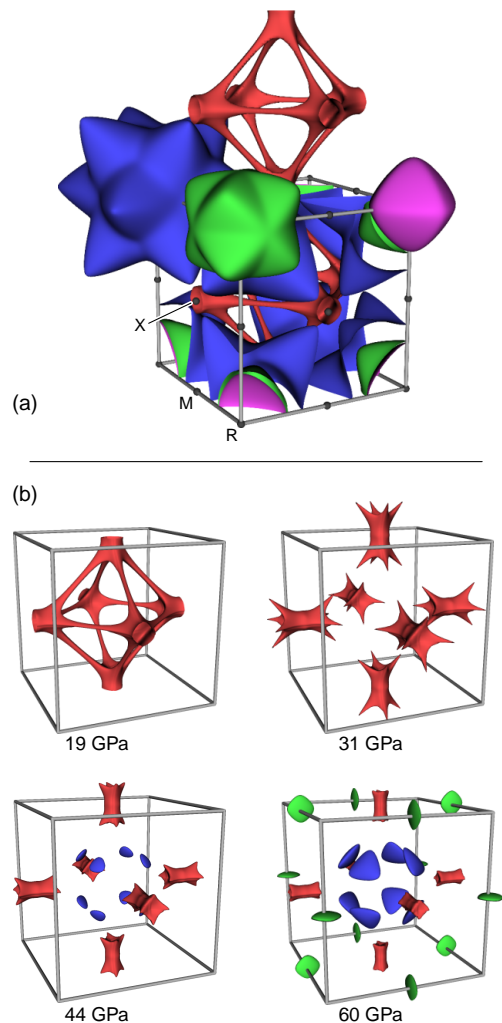


FIG. 11. (Color online) (a) Fermi surface of B2-type BiTe at a calculated pressure of 18.5 GPa (lattice parameter  $a = 3.623 \text{ \AA}$ ). (b) Evolution of the Fermi surface with pressure. The three stable pockets centered around the R point have been omitted for clarity.

level that results from the charge transfer. The calculated electron localization function for BiTe provides no evidence for any remaining covalent bonding. The chemical bonding thus changes from mixed covalent-ionic (plus van-der-Waals interactions between the layers) at normal conditions to mixed metallic-ionic at pressure of 20 GPa and above. The Fermi surface of BiTe has an intricate structure, which may give rise to interesting electron-phonon coupling effects, and it has been calculated to undergo three topological changes in the 20–60 GPa range.

*Note added.* After submission of the manuscript, Stillwell *et al.*<sup>47</sup> reported the observation of a bcc alloy phase in  $\text{Bi}_2\text{Te}$  under high pressure and that this phase is superconducting. Superconductivity is certainly an interesting example of possible electron-phonon coupling effects mentioned above. An obvious question is now how the atomic ordering reported in the present work affects the superconducting properties of cu-

bic  $\text{Bi}_m\text{Te}_n$  phases.

### ACKNOWLEDGMENTS

We thank D. L. Sun and C. T. Lin (Max-Planck-Institut für Festkörperforschung, Stuttgart) for providing the  $\text{Bi}_2\text{Te}_3$  sin-

gle crystal as well as M. Hanfland (ESRF) and A. Kleppe (DLS) for their support during the diffraction experiments. Facilities were made available by the European Synchrotron Radiation Facility and Diamond Light Source.

- \* Corresponding author: E-mail I.Loa@ed.ac.uk
- <sup>1</sup> H. J. Goldsmid, *Materials* **7**, 2577 (2014).
  - <sup>2</sup> M. A. Il'ina and E. S. Itskevich, *Fiz. Tverd. Tela* **13**, 2496 (1971), [*Sov. Phys. Solid State* **13**, 2098 (1972)].
  - <sup>3</sup> M. Einaga, Y. Tanabe, A. Nakayama, A. Ohmura, F. Ishikawa, and Y. Yamada, *J. Phys.: Conf. Ser.* **215**, 012036 (2010).
  - <sup>4</sup> J. L. Zhang, S. J. Zhang, H. M. Weng, W. Zhang, L. X. Yang, Q. Q. Liu, S. M. Feng, X. C. Wang, R. C. Yu, L. Z. Cao, L. Wang, W. G. Yang, H. Z. Liu, W. Y. Zhao, S. C. Zhang, X. Dai, Z. Fang, and C. Q. Jin, *Proc. Nat. Acad. Sci. USA* **108**, 24 (2011).
  - <sup>5</sup> C. Zhang, L. Sun, Z. Chen, X. Zhou, Q. Wu, W. Yi, J. Guo, X. Dong, and Z. Zhao, *Phys. Rev. B* **83**, 140504 (2011).
  - <sup>6</sup> K. Matsubayashi, T. Terai, J. S. Zhou, and Y. Uwatoko, *Phys. Rev. B* **90**, 125126 (2014).
  - <sup>7</sup> E. S. Itskevich, L. M. Kashirskaya, and V. F. Kraidenov, *Semiconductors* **31**, 276 (1997).
  - <sup>8</sup> M. K. Jacobsen, R. S. Kumar, A. L. Cornelius, S. V. Sinogeiken, and M. F. Nicol, *AIP Conf. Proc.* **955**, 171 (2007).
  - <sup>9</sup> A. Polian, M. Gauthier, S. M. Souza, D. M. Trichês, J. Cardoso de Lima, and T. A. Grandi, *Phys. Rev. B* **83**, 113106 (2011).
  - <sup>10</sup> J. Zhang, C. Liu, X. Zhang, F. Ke, Y. Han, G. Peng, Y. Ma, C. Gao, Y. Ma, and C. Gao, *Appl. Phys. Lett.* **103**, 052102 (2013).
  - <sup>11</sup> M. Z. Hasan and C. L. Kane, *Rev. Mod. Phys.* **82**, 3045 (2010).
  - <sup>12</sup> X.-L. Qi and S.-C. Zhang, *Rev. Mod. Phys.* **83**, 1057 (2011).
  - <sup>13</sup> R. J. Cava, H. Ji, M. K. Fuccillo, Q. D. Gibson, and Y. S. Hor, *J. Mater. Chem. C* **1**, 3176 (2013).
  - <sup>14</sup> J. R. Jeffries, A. L. Lima Sharma, P. A. Sharma, C. D. Spataru, S. K. McCall, J. D. Sugar, S. T. Weir, and Y. K. Vohra, *Phys. Rev. B* **84**, 092505 (2011).
  - <sup>15</sup> M. Einaga, A. Ohmura, A. Nakayama, F. Ishikawa, Y. Yamada, and S. Nakano, *Phys. Rev. B* **83**, 092102 (2011).
  - <sup>16</sup> L. Zhu, H. Wang, Y. Wang, J. Lv, Y. Y. Ma, Q. Cui, Y. Y. Ma, and G. Zou, *Phys. Rev. Lett.* **106**, 145501 (2011).
  - <sup>17</sup> J. W. G. Bos, H. W. Zandbergen, M.-H. Lee, N. P. Ong, and R. J. Cava, *Phys. Rev. B* **75**, 195203 (2007).
  - <sup>18</sup> J.-W. G. Bos, F. Faucheux, R. A. Downie, and A. Marcinkova, *J. Solid State Chem.* **193**, 13 (2012).
  - <sup>19</sup> H. K. Mao, J. Xu, and P. M. Bell, *J. Geophys. Res.* **91**, 4673 (1986).
  - <sup>20</sup> A. Hammersley, "computer code FIT2D," (ESRF, Grenoble, 2005).
  - <sup>21</sup> V. Petříček, M. Dušek, and L. Palatinus, *Z. Kristallogr.* **229**, 345 (2014).
  - <sup>22</sup> P. Blaha, K. Schwarz, G. K. H. Madsen, D. Kvasnicka, and J. Luitz, *Wien2k: An Augmented Plane Wave + Local Orbitals Program for Calculating Crystal Properties* (K. Schwarz, Techn. Universität Wien, Austria, 2001).
  - <sup>23</sup> Computer code ELK, version 2.3.16, <http://elk.sourceforge.net>.
  - <sup>24</sup> J. Perdew, A. Ruzsinszky, G. Csonka, O. Vydrov, G. Scuseria, L. Constantin, X. Zhou, and K. Burke, *Phys. Rev. Lett.* **100**, 1 (2008).
  - <sup>25</sup> S. K. Mishra, S. Satpathy, and O. Jepsen, *J. Phys. Condens. Matter* **9**, 461 (1997).
  - <sup>26</sup> G. A. Thomas, D. H. Rapkine, R. B. Van Dover, L. F. Mattheiss, W. A. Sunder, L. F. Schneemeyer, and J. V. Waszczak, *Phys. Rev. B* **46**, 1553 (1992).
  - <sup>27</sup> The atomic sphere radii  $R_{\text{MT}}$  were 2.5 bohr for both Bi and Te in the Wien2k calculations, and 2.8 and 2.6 bohr, respectively, in the ELK calculations. The plane wave basis set was defined by the parameter  $R_{\text{MT}}K_{\text{max}} = 9$ .
  - <sup>28</sup> A. Otero-de-la Roza, M. Blanco, A. M. Pendás, and V. Luaña, *Computer Phys. Comm.* **180**, 157 (2009).
  - <sup>29</sup> A. D. Becke and K. E. Edgecombe, *J. Chem. Phys.* **92**, 5397 (1990).
  - <sup>30</sup> A. Savin, R. Nesper, S. Wengert, and T. F. Fässler, *Angew. Chem. Int. Ed.* **36**, 1808 (1997).
  - <sup>31</sup> Y. Akahama, H. Kawamura, and A. K. Singh, *J. Appl. Phys.* **92**, 5892 (2002).
  - <sup>32</sup> C. Hejny and M. I. McMahon, *Phys. Rev. Lett.* **91**, 215502 (2003).
  - <sup>33</sup> G. Parthasarathy and W. B. Holzapfel, *Phys. Rev. B* **37**, 8499 (1988).
  - <sup>34</sup> K. Aoki, S. Fujiwara, and M. Kusakabe, *J. Phys. Soc. Jpn.* **51**, 3826 (1982).
  - <sup>35</sup> A. Nakayama, M. Einaga, Y. Tanabe, S. Nakano, F. Ishikawa, and Y. Yamada, *High Press. Res.* **29**, 245 (2009).
  - <sup>36</sup> T. Graf, C. Felser, and S. S. Parkin, *Prog. Solid State Chem.* **39**, 1 (2011).
  - <sup>37</sup> P. Kharel, W. Zhang, R. Skomski, S. Valloppilly, Y. Huh, R. Fuglsby, S. Gilbert, and D. J. Sellmyer, *J. Phys. D: Appl. Phys.* **48**, 245002 (2015).
  - <sup>38</sup> R. Cahn, *Acta Metall. Sin.* **8**, 261 (1995).
  - <sup>39</sup> K. Kobayashi, R. Y. Umetsu, R. Kainuma, K. Ishida, T. Oyamada, A. Fujita, and K. Fukamichi, *Appl. Phys. Lett.* **85**, 4684 (2004).
  - <sup>40</sup> E. S. Itskevich, S. V. Popova, and E. Y. Atabaeva, *Doklady Akademii Nauk SSSR* **153**, 306 (1963), [*Sov. Phys. - Doklady* **8**, 1086 (1964)].
  - <sup>41</sup> A. M. James and M. P. Lord, *Macmillan's Chemical and Physical Data* (Macmillan, London, 1992).
  - <sup>42</sup> R. F. W. Bader, *Chem. Rev.* **91**, 893 (1991).
  - <sup>43</sup> R. F. W. Bader, *Atoms in Molecules: A Quantum Theory* (Clarendon Press, Oxford, 1990).
  - <sup>44</sup> C. A. Kagarakis, *J. Mater. Sci.* **13**, 1594 (1978).
  - <sup>45</sup> P. Pecheur and G. Toussaint, *Phys. Lett. A* **135**, 223 (1989).
  - <sup>46</sup> T. Sugimoto, Y. Akahama, T. Ichikawa, H. Fujihisa, N. Hirao, and Y. Ohishi, *J. Phys.: Conf. Ser.* **500**, 192018 (2014).
  - <sup>47</sup> R. L. Stillwell, Z. Jenei, S. T. Weir, Y. K. Vohra, and J. R. Jeffries, *Phys. Rev. B* **93**, 094511 (2016).